Results and Discussion

CHAPTER 4

Development of a cost-effective, recyclable and viable metal ion doped adsorbent for simultaneous adsorption and reduction of toxic Cr (VI) ions

Chapter 4: Development of a cost-effective, recyclable and viable metal ion doped adsorbent for simultaneous adsorption and reduction of toxic Cr (VI) ions

4.1 Introduction

The Cr (VI) is more soluble in water compared to Cr (III). Hence, adsorption of Cr (VI) followed by reduction into Cr (III) is considered beneficial in its adsorption [Bandara et al., 2020]. Chemical agents such as sodium dithionite, H_2O_2 and Fe (II) etc., have been used as reducing agent [Gao and Liu, 2017]. Among these reducing agents, Fe (II) ion has been considered as highly effective and non-toxic. There are several studies on iron doped adsorbent which have been conducted for Cr (VI) ion removal. Wang et al., 2020c carried out adsorption of Cr (VI) by using iron loaded carbon. Verma et al., 2015 synthesized iron-loaded resorcinol formaldehyde-based aerogels for Cr (VI) removal. The drawback of these studies was their complex procedure of adsorbent preparation, non-eco-friendly nature and time-consuming processing and expensiveness.

This study focuses on the development of a cost-effective, recyclable and viable Cr (VI) ion adsorbent for simultaneous adsorption and reduction from agro-waste (rice husk) doped with Fe (II) ions (FeRH). Rice husk is a waste product generated from rice mill and is easily and readily available worldwide. The synthesized adsorbent was characterized using several techniques such as SEM-EDX, FTIR, BET, Proximate and ultimate analysis and pH_{pzc}. XPS analysis was conducted to confirm the reduction of Cr (VI) to Cr (III). ANN feed-forward back propagation algorithm is used for the modeling of Cr (VI) on undoped rice husk (RH) and FeRH. Dimensionless numbers are derived and calculated to explore the adsorption of Cr (VI) ions in the liquid phase. The uptake capacities of FeRH and RH and thermodynamic feasibility of adsorption were estimated by using standard kinetic, isotherm and thermodynamic models. The viability of FeRH was explored in terms of repeated adsorption hysteresis. Finally, to show the applicability of this adsorbent, a comparative study with other adsorbents has been done

and the guidelines of Cr (VI) permissible level of discharge as prescribed by WHO, USA and CPCB, India are satisfied.

4.2 Characterization of FeRH and RH

4.2.1 SEM analysis

As shown in the Figure 4.1a, the surface of RH was found uneven and irregular before adsorption. The surface of RH exhibited many cone and villi-like structure between two-line framework. This distinctive structure of RH provides tremendous surface which makes it a quality adsorbent. After iron doping, modified rice husk (FeRH) became more rough, porous with enhanced irregularity (Figure 4.1c). Figure 4.1 b and d indicated the presence of even and regular structures in Cr (VI) loaded RH and FeRH.

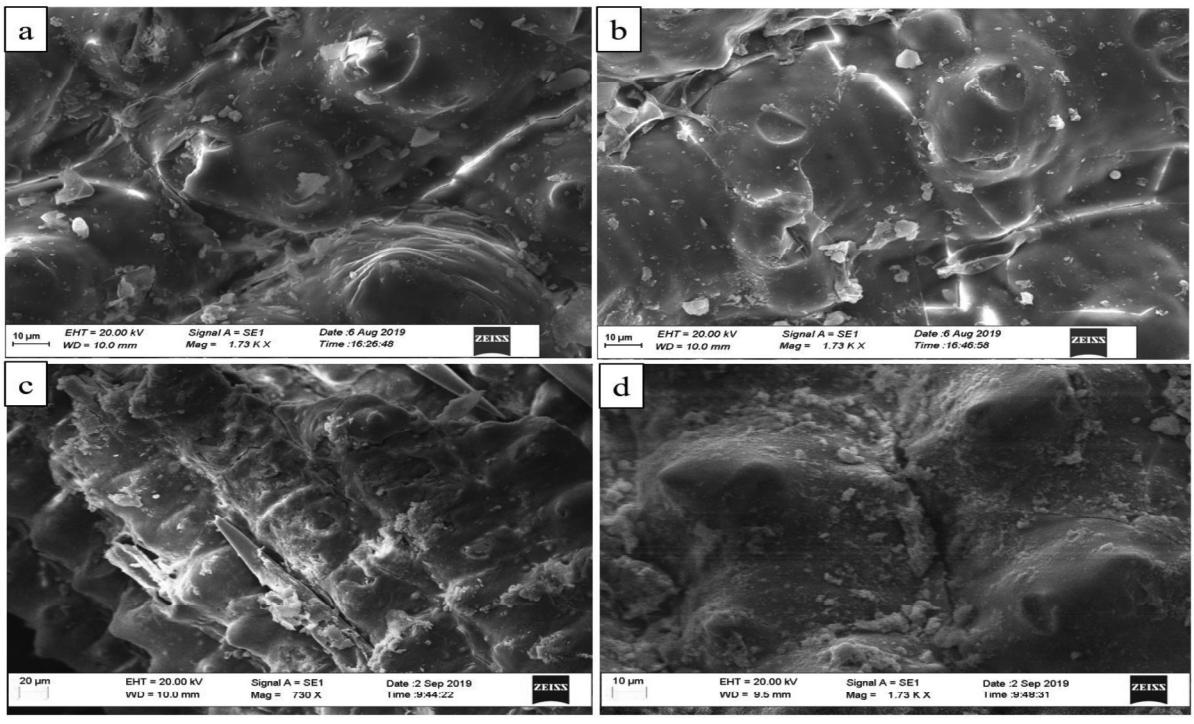

Figure 4.1. SEM image of (a) unloaded RH (b) metal loaded RH (c) unloaded FeRH (d) metal loaded FeRH

These changes were attributed to the binding of Cr (VI) in the pores and grooves present on the surface of RH and FeRH. Zhang et al., 2014 performed the biosorption of copper (II) onto H_3PO_4-treated rice husk and Genieva et al., 2008 characterized rice husk and its products. Both researchers found morphology of RH similar to the results reported in the present study.

4.2.2 EDX analysis

Adsorption of Cr (VI) on the surface of RH and FeRH was confirmed through EDX spectra (Figure 4.2a-d).

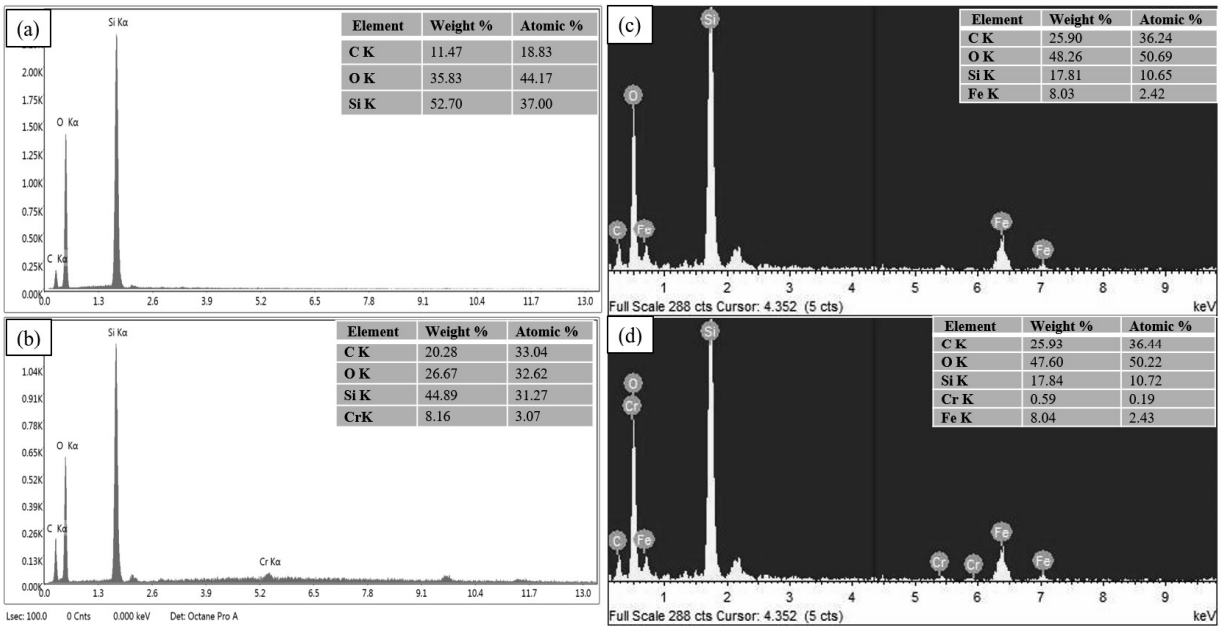

Figure 4.2 EDX spectra of (a) unloaded RH (b) metal loaded RH (c) unloaded FeRH (d) metal loaded FeRH

It was observed that RH was composed of silica, carbon and oxygen (Figure 4.2 a). The large amount of chromium was also observed on the surface of RH after adsorption (Figure 4.2 b). The presence of iron on the surface of FeRH proved the efficacious iron doping on RH surface (Figure 4.2 c). EDX spectra (Figure 4.2 d) assured the occurrence of chromium along with other major elements on FeRH surface. Zhang et al., 2014 performed XRF analysis of rice

husk and reported large amount of silica in the rice husk, which is a key player in the adsorption of heavy metal ions. Irfan et al., 2014 did EDX analysis of iron doped carbon material and reported iron binding on the surface of activated carbon after doping.

4.2.3 FTIR

Figure 4.3 shows the FTIR spectra of RH and FeRH before and after the Cr (VI) adsorption.

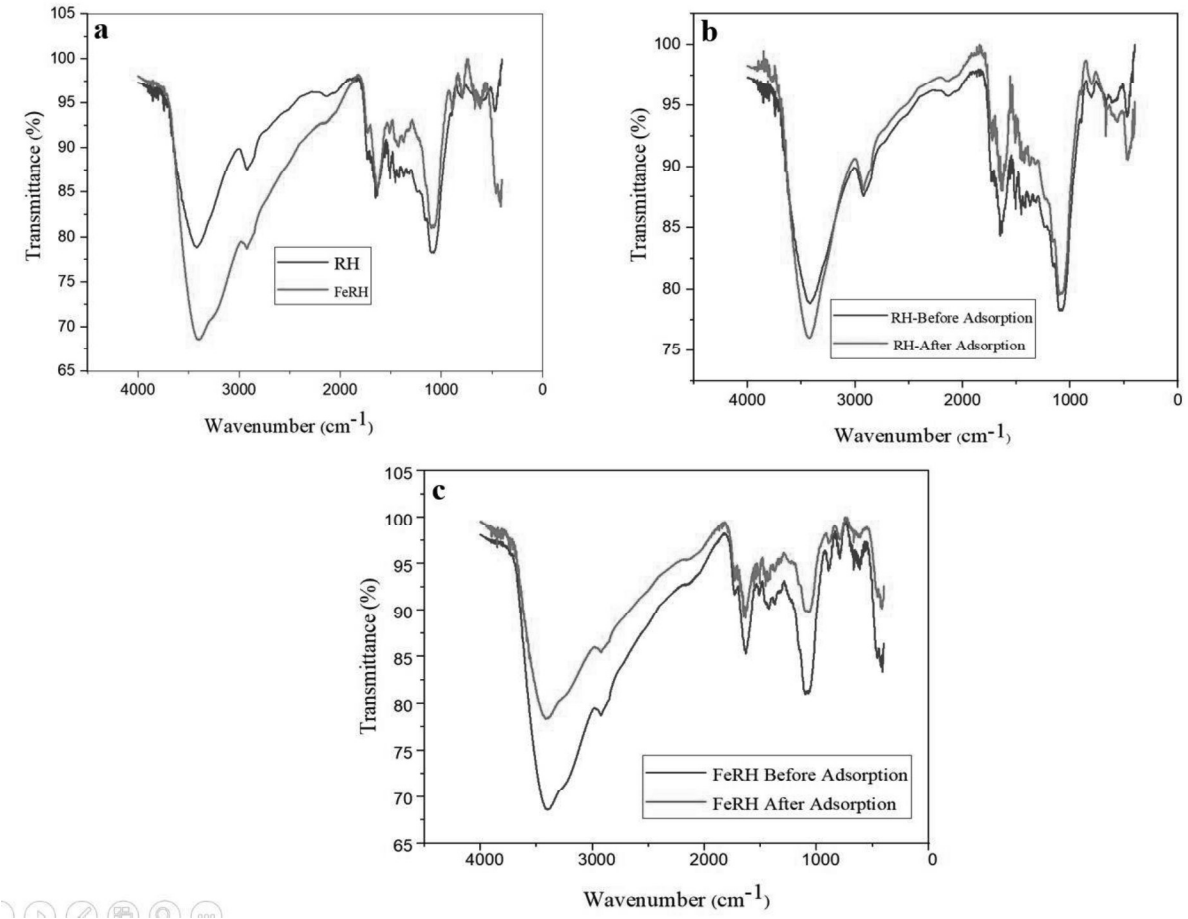

Figure 4.3 FTIR spectra of (a) RH and FeRH (b) metal unloaded and loaded RH (c) metal unloaded and loaded FeRH

The broad peaks between 3000 and 3800 cm^{-1} showed the –OH and –NH moieties on the unloaded RH and FeRH (Figure 4.3 a). In Cr (VI) loaded RH and FeRH shifting of the bands was observed (Figure 4.3 b and c). It has been reported that the adsorption of heavy

metals usually occurs between the range of 3200 and 3500 cm^{-1} due to the presence of –OH and –NH functional groups [Akal et al., 2009]. The peaks at 2714 cm^{-1} in RH and FeRH were attributed to the stretching of C–H bonds of methylene ring and alkane groups [Kibami et al., 2017]. The C≡C vibrations (aromatic ring phase) were observed between 1500 and 1700 cm^{-1} [Xu et al., 2013]. The peaks at 1395 cm^{-1} were due to the vibration of –CH–(CH_3) [Quintelas et al., 2013].

The peaks between 1000 and 1100 cm^{-1} depicted the presence of C– OH in carboxyl and alcohol groups [Long et al., 2014]. The shifting of peaks between 900 and 400 cm^{-1} in RH and FeRH indicated the changes in the adsorbent surface after iron doping and chromium adsorption. Saha et al., 2013 and Quintelas et al., 2013 testified similar type of functional groups and reported suitability of these functional groups in adsorption of Cr (VI) and other inorganic pollutants present in the contaminated water.

4.2.4 Proximate and ultimate analysis

The moisture, ash, volatile matter, carbon, hydrogen, oxygen, nitrogen and sulfur content in RH and FeRH are listed in Table 4.1.

Table 4.1. Proximate and ultimate analysis of RH and FeRH

Ultimate analysis	**Weight %**	
	RH	**FeRH**
Moisture	6.23	5.88
Ash	22.01	22.49
Volatile matter	60.67	59.31
Fixed carbon	11.09	12.32
Proximate analysis		

C	35.59	36.12
H	7.21	6.01
O	38.09	38.19
N	0.42	0.41
S	0.02	0.03

The low moisture content in FeRH assists in the adsorbent preparation with enhanced shelf-life. Adsorbents with low moisture content also require less drying time before getting used in the experiments [Kamsonlian et al., 2012]. The high C, H and O content together with functional groups like carboxyl, hydroxyl in FeRH rendered momentous uptake capacity for Cr (VI) ions. These functional groups are actively involved in the heavy metal ion adsorption. Dawodu et al., 2020 reported the fixed carbon in *Heinsia crinita* seed coat biomass as 70.40% and 68.30% from proximate and ultimate analysis. Authors reported that due to high carbon content in *Heinsia crinite* biomass, it is considered as a good biosorbent. Kapur et al., 2013 performed proximate and ultimate analysis of *Mangifera indica* sawdust and reported fixed carbon content as 16.28%. The study suggested that enormous carbon and lower moisture was suitable for storage of biosorbent for long period of time coupled with high uptake capacity.

4.2.5 pHpzc

In the present study pH_{pzc} was recorded as 3.32 (Figure 4.4).

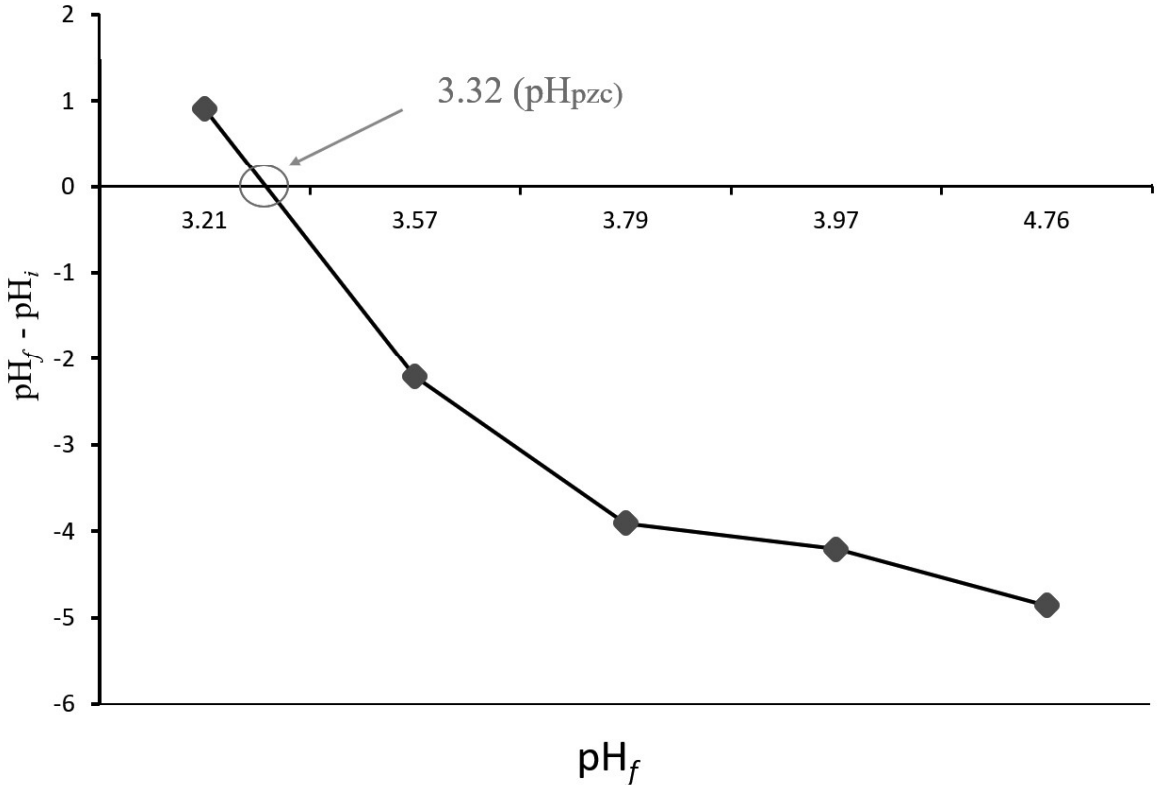

Figure 4.4 pH_{pzc} value of FeRH

It is evident from Figure 4.4 that the FeRH surface was positively charged pH < 3.32. This indicated the preferential adsorption of Cr (VI) ions at lower pH values on FeRH (pH 2 in this work). The positively charged surface of FeRH attracted the negatively charged $HCrO^{4-}$ ions which is the predominant specie of Cr (VI) ion at acidic pH [Mondal and Chakraborty, 2020]. Yusuff, 2019 projected the pH_{pzc} of activated carbon obtained from *Leucaena leucocephala* seed pod as 5.20.

4.2.6 BET surface area

A comparative analysis of specific surface area of RH and FeRH with other biosorbent is shown in Table 4.2.

Table 4.2. Specific surface area of FeRH, RH and other adsorbents

Adsorbents	**BET surface area (m^2/g)**	**References**
Modified pine bark	0.4340	[Zhang and Leiviska, 2020]
Alkali treated *Metroxylon* spp. Biomass	78.48	[Amode et al., 2016]
Pongamia pinnata shells Biosorbent	4.02	[Patra et al., 2020]
Cork powder	3.03	[Sfaksi et al., 2014]
Chemically treated rice husk	13	[Hoyos-Sanchez et al., 2017]
Burnt potato peels	13.43	[El-Azazy et al., 2019]
Rice husk Char	141	[Paethanom and Yoshikawa, 2012]
Modified pomelo peel's pulp	36.733	[Yang et al., 2019]
RH	7.05	This study
FeRH	75.31	This study

It became apparent from Table 4.2 that FeRH has higher specific area as compared to RH and most of the adsorbents developed in other investigations. The surface area of the rice husk was found lower than Fe doped rice husk. The reason behind this, the surface of Fe doped rice became more porous and rough as compared to un-doped rice husk. Enhanced roughness and pores on Fe doped rice husk were responsible for higher surface area.

4.3.0 Dimensionless numbers

Table 4.3 shows the value of dimensionless numbers (φ, λ and N_k).

Table 4.3 Dimensionless numbers for RH and FeRH

Adsorbent	φ	λ	N_k
RH	62.29×10^{-2}	4.06×10^{-3}	1.22×10^{3}
FeRH	78.9×10^{-2}	1.66×10^{-3}	1.98×10^{3}

The N_k ranged from 101 to 104, which infers that diffusion dominated the adsorption. The value of φ and λ were between 10^{-2} to 10^{4} and 10^{-12} to 10^{8}, respectively. This reflected broad surface exposure with minimal surface tension throughout the adsorption [Ferri et al., 2001]. Singh and Mishra, 2020 utilized dimensionless numbers while modeling adsorption flux of nickel contaminated water in the batch system and found that initially adsorption was controlled by film diffusion followed by intraparticle at the later stage.

4.4.0 ANN

The analysis of predicted and test results yielded a high level of linear regression (R^2 = 0.81 and 0.94) for RH and FeRH, respectively, which implied that the proposed model was able to accurately predict the efficacy of adsorption appropriately for FeRH but not for RH. The lowest mean squared error (MSE) for data sets was achieved at epoch 16 and 15 (Figure 4.5).

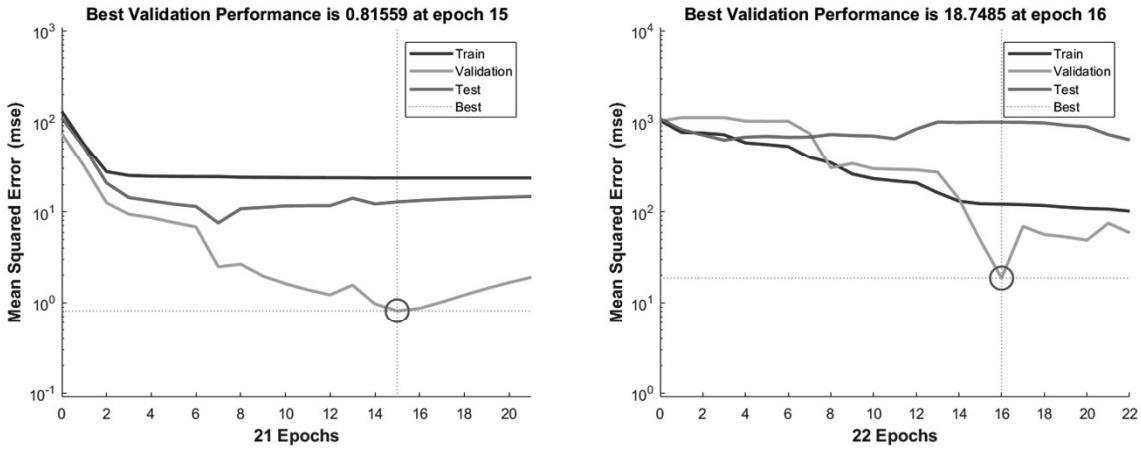

a) **b)**

Figure 4.5 Performance plot of (a) RH and (b) FeRH

The best validation performance was observed at 18.74 and 0.81 in ten neurons for RH and FeRH, respectively. Correlation plots between experimental and predicted values are shown in Figure 4.6 for further verification of result.

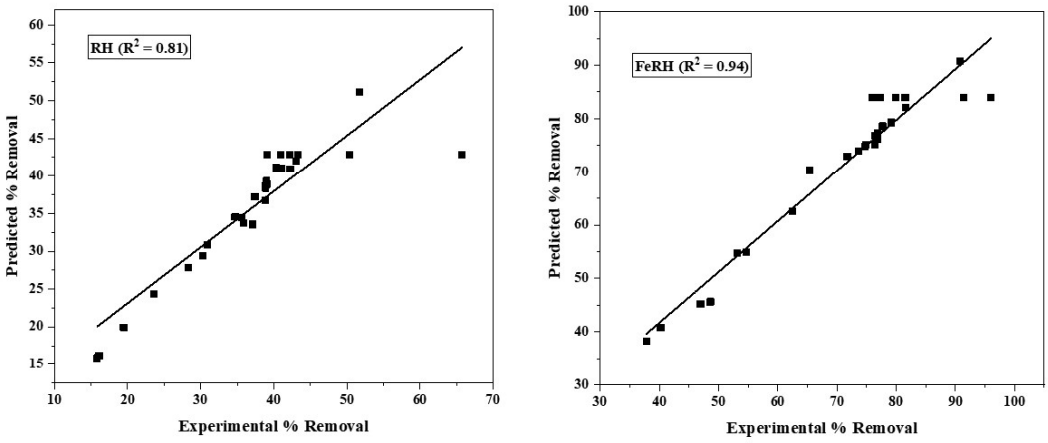

a) **b)**

Figure 4.6 Comparison of predictive and experimental values for (a) RH and (b) FeRH using ANN

Only 1.32% and 0.18% of variance in RH and FeRH was observed in the experimental values when compared with ANN predicted one. This showed that the ANN model was able to precisely predict the percentage removal of Cr (VI) by RH and FeRH with R^2 = 81 for RH

and R^2 = 0.94 for FeRH with MSE > 10 for RH and MSE = 1 for FeRH. These results were more reasonable and appropriate for FeRH in comparison to RH. Similarly, Singha et al., 2014 applied ANN modeling for adsorption of Cr (VI) by using various biosorbents and found that the percentage removal of Cr (VI) ions from the aqueous solution was accurately predicted by a single hidden layer trained with L-M algorithm. Sen et al., 2018 developed an ANN model for biosorption of Cr (VI) onto cyanobacterial biomass and reported that the model has adequate generalization with fair precision for unseen experimental data.

4.5.0 Conformity of oxidation state

Results of XPS analysis confirmed the presence of Fe, Cr, O, Si and C (Figure 4.7).

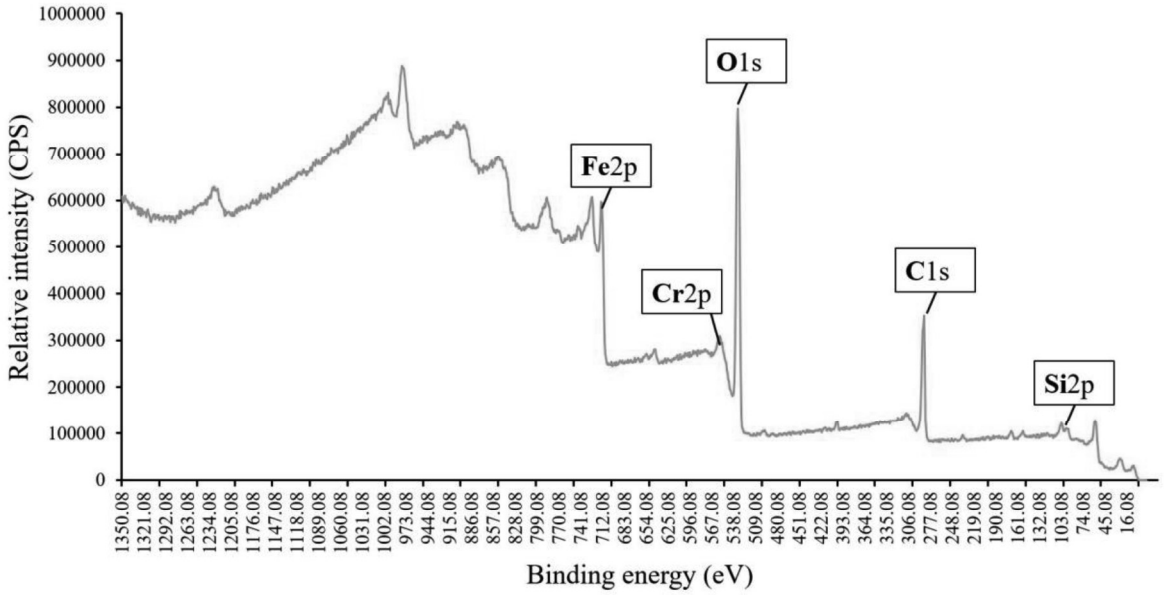

Figure 4.7 XPS analysis of Cr (VI) loaded FeRH

The presence of iron in the FeRH confirmed the efficacious iron coating on the rice husk. C and Si were also observed in the XPS as they are major structural components of rice husk [Fernandes et al., 2016]. The presence of chromium indicated the successful adsorption

on the surface of FeRH. The chromium oxidation states on to FeRH surface is shown in Figure 4.8.

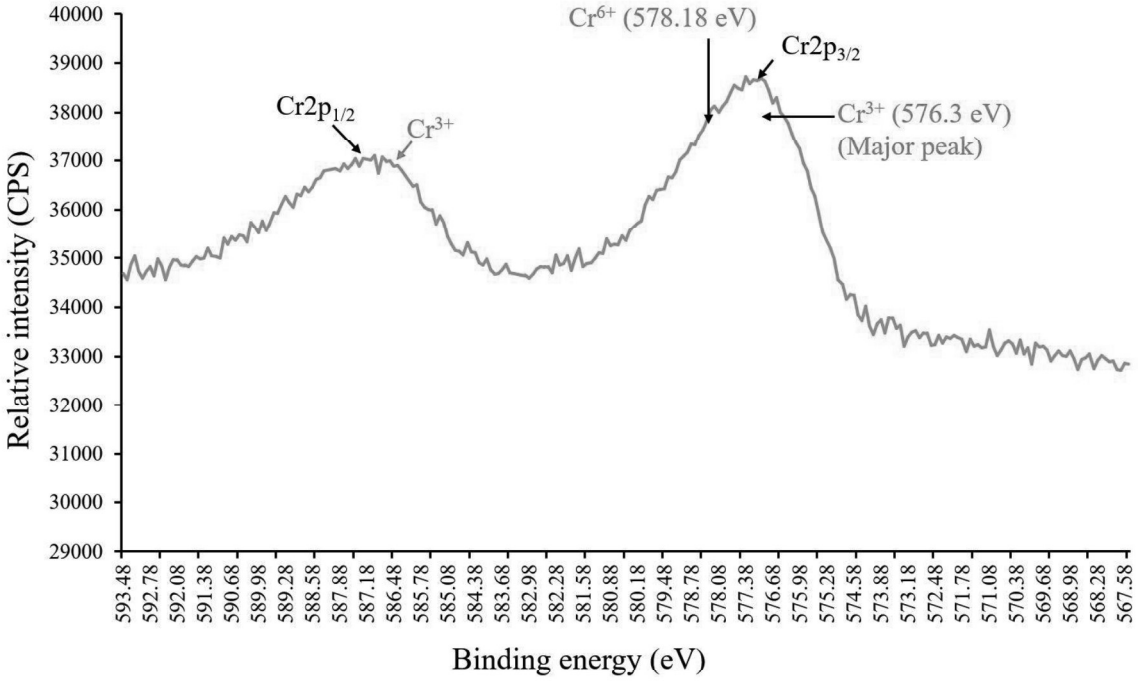

Figure 4.8 Oxidation state of adsorbed Cr on to FeRH

XPS spectra was collected from the Cr2p domain of the FeRH. The significant bands of Cr (III) appeared at 577.0–579.0 and 586.5–588.0 eV corresponding to Cr2p3/2 and Cr2p1/2 orbital, respectively [Park et al., 2007]. The insignificant Cr (VI) peaks appeared at 579.0–581.0 and 588.5–590.0 eV [Park et al., 2007]. These results indicated that chromium bound to the surface of FeRH was mostly in trivalent state. Dupont and Guilon, 2003 reported that adsorption consumed substantial proportion of protons, which was responsible for reduction of Cr (VI) to Cr (III) during biosorption on the surface of lignocellulosic extract of wheat bran. The authors reported that oxidation of lignin occurred during the reduction of Cr (VI). Aranda-Garcia and Cristiani-Urbina, 2020 reported Cr (VI) biosorption using *Quercus crassipes* shell. Authors investigated mechanism of Cr (VI) removal by using XPS analysis and found that most of adsorbed chromium was in the trivalent state.

4.6.0 Proposed mechanism: surface protonation, adsorption and reduction

Between pH 2 and 6, the Cr (VI) ions exist as negatively charged chromate ion ($HCrO^{4-}$) (Park et al., 2005). At such a low pH, concentration of hydrogen ions is too high in the solution and this leads to extensive protonation of amino and carboxyl groups on FeRH surface. These protonated groups together with doped Fe^{2+} ions not only attract (adsorb) the $HCrO^{4-}$ ions but also reduces them into Cr (III) [Saha et al., 2010; Park et al., 2005]. The doping of Fe^{2+} ions significantly enhances the rate of Cr (VI) adsorption-cum-reduction into Cr (III) as compared to undoped RH.

The reduction mechanism is as follows:

$$Fe^{2+} \rightarrow Fe^{3+} + e^{-} \quad (37)$$

$$3\,Fe^{2+} \rightarrow 3\,Fe^{3+} + 3\,e^{-} \quad (38)$$

$$Cr_2O_7^{2-} + 14\,H^{+} + 6\,e^{-} \rightarrow 2\,Cr^{3+} + 7\,H_2O \quad (39)$$

In the reduction of Cr (VI) to Cr (III), three moles of Fe^{2+} are required to reduce one mole of Cr (VI) to Cr (III).

4.7.0 Adsorption study

4.7.1 Effect of process parameters

4.7.1.1 pH

Cr (VI) has several stable species such as CrO_4^{2-}, $HCrO_4^{-}$ and $Cr_2O_7^{2-}$ at acidic pH. In the present investigation, maximum adsorption of Cr (VI) was observed at pH 2 which was attributed to tremendous protonation of the RH and FeRH surface (Figure 4.9c). The pronated surface attracted negatively charged chromium ions. Saha et al., 2013 performed the biosorption experiment of Cr (VI) on the surface of CLP powder and observed maximum biosorption of Cr (VI) at pH 2. Patra et al., 2019 also investigated Cr (VI) adsorption onto raw,

acid treated and chelated-activated biomass of *Sterculia villosa* Roxb Shells and reported maximum Cr (VI) removal at pH 2. Both the authors reported that at acidic pH (pH 2) the surface of biosorbent was heavily protonated which created an electrostatic pull between the negatively charged Cr (VI) species and surface active sites. This resulted in a favourable biosorption.

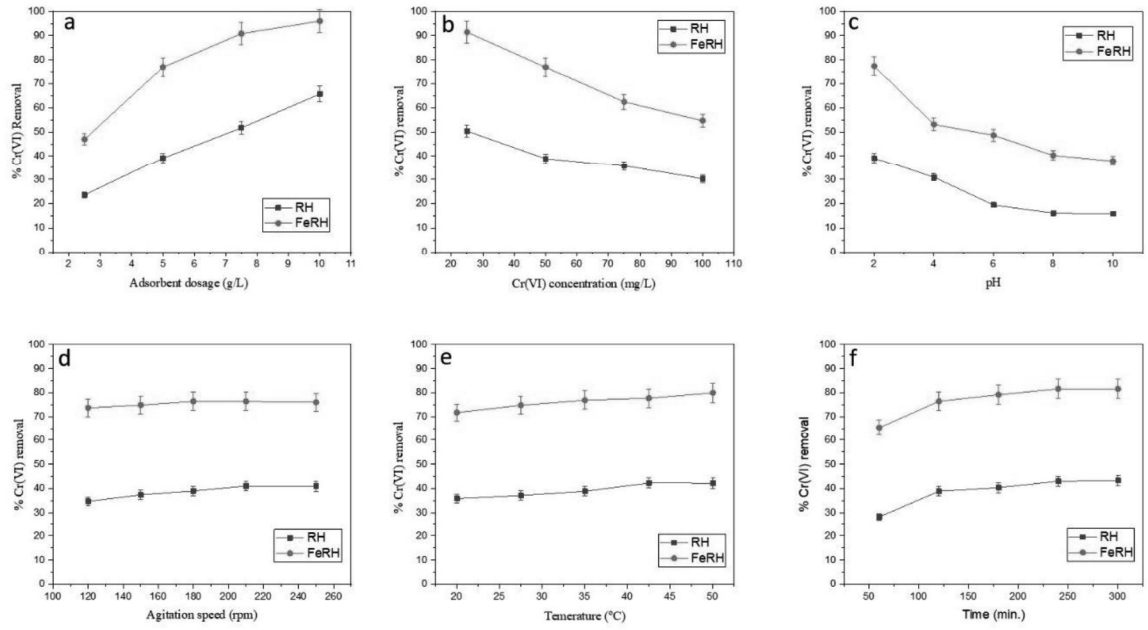

Figure 4.9 Effect of various adsorption parameters such as adsorbent dosage (a), initial Cr (VI) concentration (b), pH (c), agitation rate (d), temperature (e) and contact time (f) for Cr (VI) adsorption onto RH and FeRH.

4.7.1.2 Initial metal ion concentration

In the present work, maximum removal of Cr (VI) was found at 25 mg/L (Figure 4.9b). The percentage removal of Cr (VI) decreased with the rise in initial concentration from 25 to 100 mg/L. This was attributed to fact that the available surface area of FeRH and RH was limited and got completely occupied by Cr (VI) ions at 25 mg/L. As no surface area was available above 25 mg/L, the ions remained in the solution [Caglar et al., 2013]. The similar observations were also reported in Cr (VI) adsorption on walnut shell-based activated carbon [Ghasemi et al., 2015]. Fernandez-Lopez et al., 2014 reported that the maximum Cr (VI)

biosorption on the surface of *Opuntia* was obtained at 10 mg/L. Above 10 mg/L, authors also observed that there was decrease in the removal of Cr (VI) ions.

4.7.1.3 RH and FeRH dosage

The removal of Cr (VI) increased from 23.62 to 65.76 % and 76.88 to 96.04 % for RH and FeRH, respectively with increase in the dose from 2.5 to 10 g/L (Figure 4.9 a). This indicated that increased dose provided more surface area and enhanced adsorption sites for the binding of Cr (VI) ions. However, above 10 g/L of RH and FeRH dose, there was significant decrease in removal of Cr (VI) ions. The rationale behind this decrease was the agglomeration of RH and FeRH above 10 g/L. Bermudez et al., 2012 performed Cr (VI) removal experiment using *Sargassum muticum* brown alga and reported that biosorption is highly dependent on dose of biosorbent up to a certain level. Patra et al., 2020 also reported that Cr (VI) removal was increased up to 98% with the increase in biosorbent dose (acid-modified *Pongamia pinnata* shells biomass) from 0.4 to 4 mg/L.

4.7.1.4 Contact time

In the present work, the maximum adsorption of Cr (VI) ions was observed at 240 minutes and afterwards the removal of Cr (VI) was constant for both RH and FeRH (Figure 4.9f). This trend of contact time with removal of Cr (VI) was attributed to the fact that all the active sites on the RH and FeRH surface were saturated at 240 minutes and hence no or negligible adsorption took place thereafter. Saha et al., 2013 carried out Cr (VI) biosorption at various time interval ranging from 20 to 200 minutes and achieved equilibrium at 120 minutes. The similar observation were also reported by Mutongo et al., 2014 on Cr (VI) using potato peels powder. Panda et al., 2017 reported that Cr (VI) adsorption on industrial waste increased with the increase in contact time.

4.7.1.5 Temperature

In the present work, it was observed that the removal of Cr (VI) increased with the rise in temperature from 20 to 50 °C and the maximum removal was obtained at 50°C (Figure 4.9e). Above 50 °C, there was decrease in removal of Cr (VI) ions from the liquid phase. The rise in removal of Cr (VI) ion with increase in temperature up to 50 °C showed the endothermic profile of the adsorption coupled with generation of new adsorption sites due to breakage of internal bonding in the RH and FeRH. Above 50 °C, the adsorption was exothermic and this was due to deactivation of active sites on higher temperatures. Singh et al., 2005 reported the rise in adsorption of Cr (VI) ion with elevation in temperature from 20 to 40 °C. Authors also reported that above 40 °C there was reduction in adsorption of Cr (VI) ions. Mohapatra et al., 2009 also investigated heavy metal removal using NALCO plant sand and reported that the removal of heavy metal ions increased with the increase in reaction temperature.

4.7.1.6 Agitation speed

In the present investigation, it was observed that Cr (VI) removal improved with rise in agitation rate from 120 to 250 rpm (Figure 4.9 d). This was due to increases in the turbulence between FeRH and RH particle and metal ions together with decrease in the thickness of boundary layer around the RH and FeRH. Beyond this agitation rate, there were no further increase in the removal of Cr (VI). Similar trends in biosorption of Cr (VI) on the excess municipal sludge was reported by Mohamadi et al., 2015. Mishra et al., 2015 investigated the Cr (VI) removal using *Portulaca oleracea* biomass and reported that Cr (VI) adsorption gradually increased with the elevation in agitation speed up to 350 rpm.

4.7.2.0 Isotherm study

The isotherm study of RH and FeRH is shown in Figure 4.10 and 4.11, respectively.

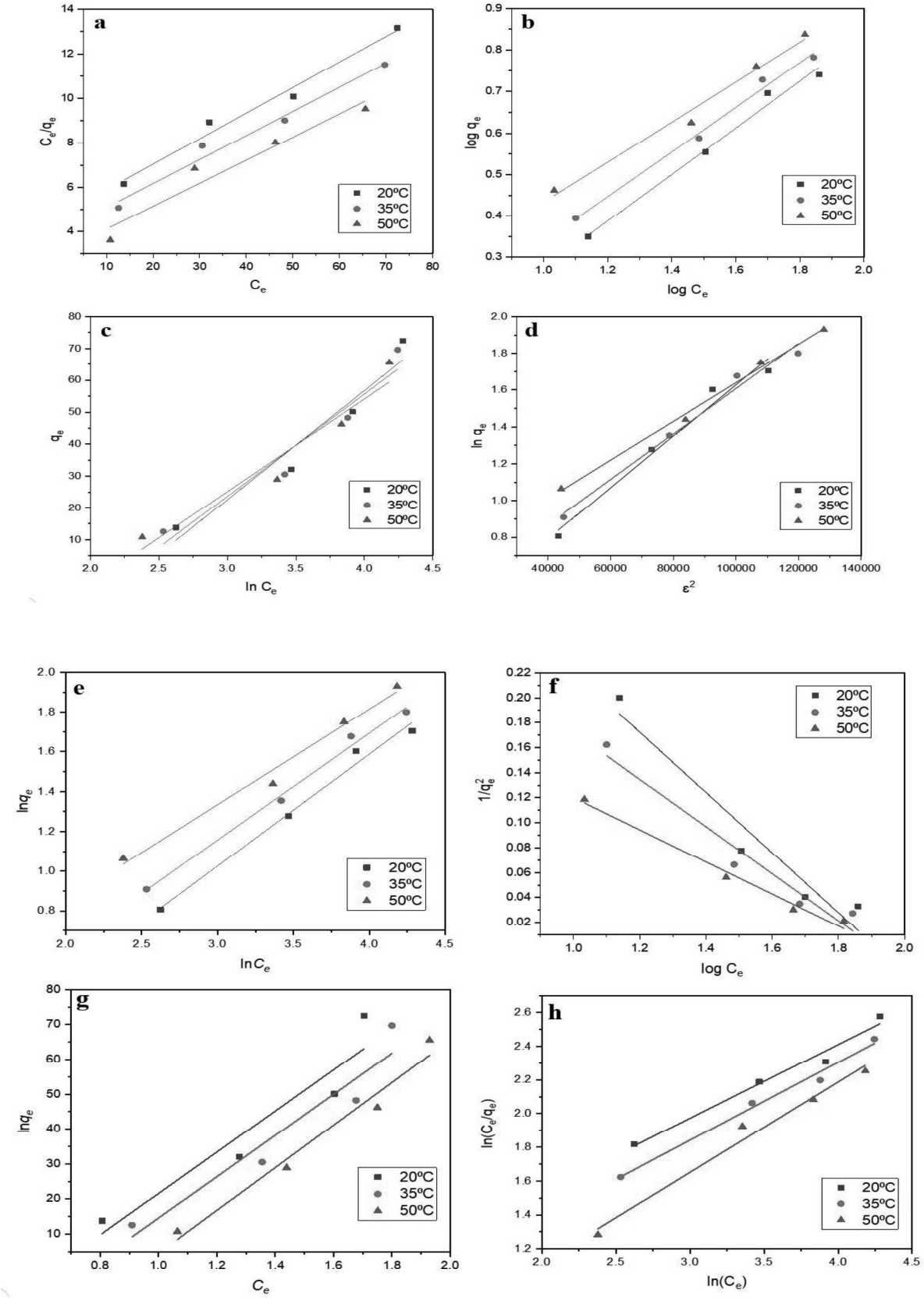

Figure 4.10 Langmuir (a), Freundlich (b), Temkin (c), D-R (d), Halsey (e), H-R (f), Jovanovic (g) and R-P isotherm of Cr (VI) adsorption onto RH.

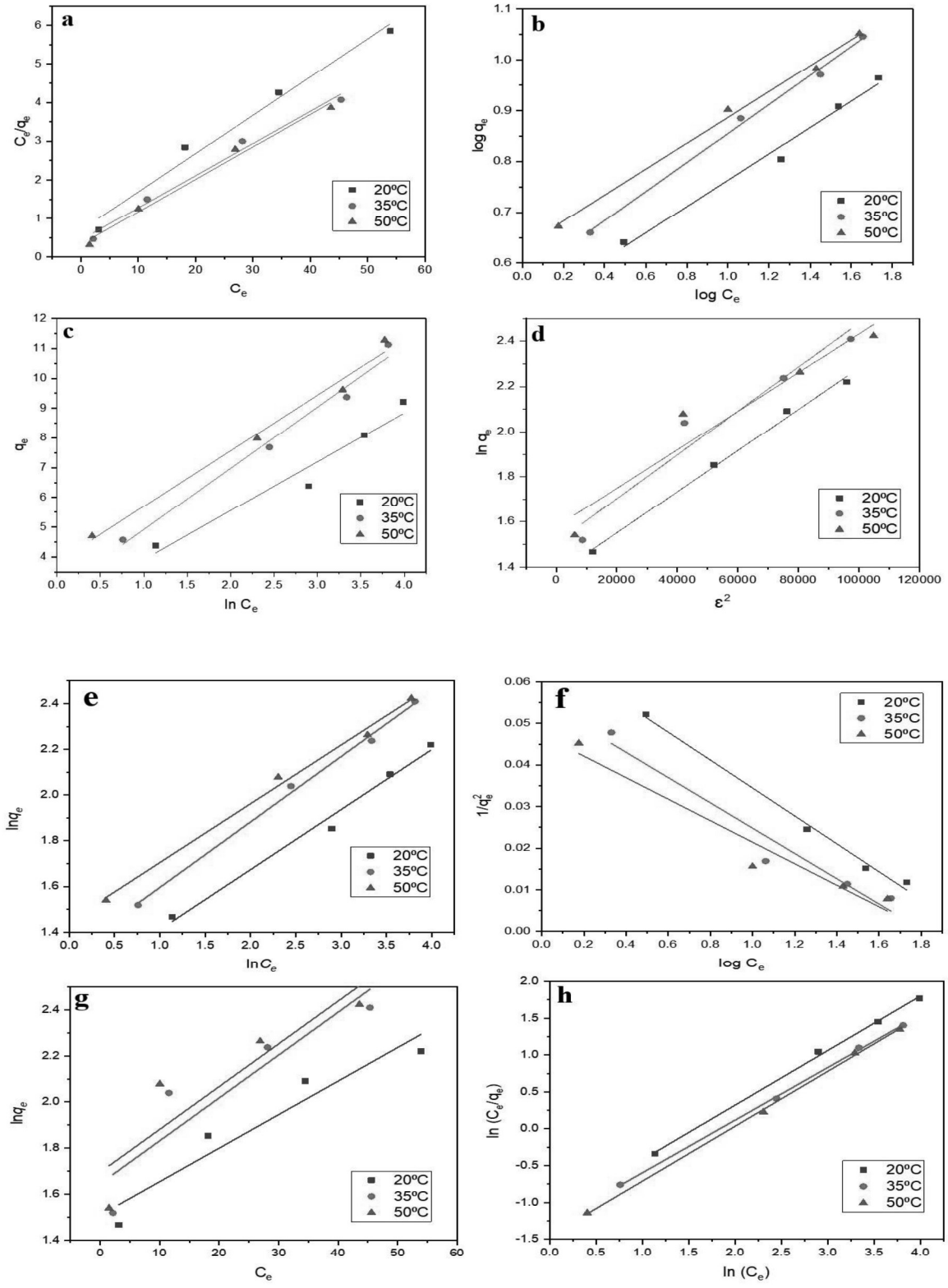

Figure 4.11 Langmuir (a), Freundlich (b), Temkin (c), D-R (d), Halsey (e), H-R (f), Jovanovic (g) and R-P isotherm of Cr (VI) adsorption onto FeRH.

The parameters of isotherm modeling calculated from graphs and shown in Table 4.4.

Table 4.4 Isotherms parameters and constants

Isotherm		RH			FeRH		
		20°C	**35°C**	**50°C**	**20°C**	**35°C**	**50°C**
Langmuir	B	4.75	4.01	3.06	0.70	0.44	0.33
	Q^0	0.11	0.11	0.10	0.09	0.08	0.08
	R^2	0.97	0.97	0.91	0.97	0.98	0.98
	SSE	0.47	0.45	1.09	9.19	3.27	4.32
	χ^2	0.16	0.15	0.36	3.06	1.09	1.44
Freundlich	k_f	-0.28	-0.19	0.04	0.50	0.56	0.63
	N	0.56	0.54	0.48	0.25	0.28	0.28
	R^2	0.99	0.99	0.99	0.99	0.99	0.99
	SSE	0.0011	0.0018	0.0012	0.019	0.027	0.016
	χ^2	0.0004	2.39	0.0004	3.06	1.09	1.44
Temkin	A_T	-79.57	-72.23	-61.75	2.26	2.85	3.82
	b_T	34.07	31.96	28.96	1.64	2.06	1.87
	R^2	0.91	0.91	0.90	0.93	0.97	0.97
	SSE	108.62	107.36	106.60	0.63	0.36	0.32
	χ^2	36.20	35.78	35.53	0.21	0.12	0.10
D-R	$Q_{D\text{-}R}$	0.23	0.38	0.59	1.37	1.50	1.57
	β	1.39	1.23	1.05	9.13	9.71	8.54
	R^2	0.96	0.97	0.99	0.99	0.92	0.89
	SSE	0.012	0.0074	0.0018	0.0015	0.021	0.031
	χ^2	0.004	0.0024	0.0006	0.0005	0.007	0.01

Halsey	K_H	0.56	0.53	0.48	0.26	0.28	0.25
	n_H	-0.66	-0.45	-0.10	1.15	1.31	1.44
	R^2	0.99	0.99	0.98	0.99	0.99	0.99
	SSE	0.006	0.0036	0.0067	0.0043	0.0017	0.0025
	χ^2	0.002	0.002	0.0022	0.0014	0.0005	0.0008
H-J	*B*	-0.24	-0.19	-0.12	-0.03	-0.03	-0.02
	A	0.46	0.36	0.25	0.07	0.05	0.04
	R^2	0.94	0.92	0.98	0.99	0.92	0.91
	SSE	0.0011	5.56	8.46	7.16	5.30	4.86
	χ^2	0.0003	1.85	2.82	2.38	1.76	1.62
Jovanovic	q_e	58.95	59.00	60.99	0.01	0.01	0.01
	q_{max}	-37.33	-44.40	-56.41	1.51	1.64	1.69
	R^2	0.90	0.92	0.97	0.92	0.84	0.81
	SSE	184.42	138.61	46.60	0.025	0.070	0.08
		61.47	46.20	15.53	0.008	0.023	0.026
R-P	β	0.44	0.46	0.54	0.74	0.71	0.74
	A	0.66	0.45	0.043	-1.16	-1.30	-1.45
	R^2	0.98	0.99	0.98	0.99	0.99	0.99
	SSE	0.0059	0.0039	0.0093	0.0046	0.0017	0.0022
	χ^2	0.0019	0.0013	0.0031	0.0015	0.0005	0.0007

The greater R^2 and diminished values of χ^2 and SSE for Freundlich isotherm relative to other isotherms revealed that adsorption of Cr (VI) onto FeRH and RH was in multilayer on the heterogeneous surface [Chaudhry et al., 2016]. The adsorption was favorable at high temperature as the value of n ranged from 0.56 to 0.48 for RH and from 0.25 to 0.28 for FeRH

and there was a surge in value of k_f from 0.503 to 0.631 mg/g with increase in temperature from 20 to 50 ºC. In present work, the value of Langmuir constant Qº decreased with escalation in temperature. This model failed in goodness-of-fit of the experimental data [Chaudhry et al., 2016]. A_T values of Temkin isotherm increased with the stepping-up of temperature from 20 to 50 ºC, which signified strong binding between Cr (VI) and adsorbent. Theoretical saturation coefficient Q_{D-R} of D-R isotherm improved from 0.2361 to 0.4905 for RH and 1.3686 to 1.5780 for FeRH with temperature uplift. This again indicated that the binding between Cr (VI) and RH and FeRH was endothermic.

The free energy (E) calculated from equation of D-R isotherm were 0.599, 0.637, 0.694 kJ mol^{-1} for RH and 0.234, 0.227, 0.242 kJ mol^{-1} for FeRH (< 8.0 kJ mol^{-1}). These observations indicated that the adsorption was physical in nature for both RH and FeRH [Mishra et al., 2009; Rao et al., 2014]. Higher R^2 values were also reported in H-J isotherm, which complemented the finding that Cr (VI) adsorption was in multilayer fashion on heterogeneous surface. Jovanovic isotherm did not fit well which ruled out the possibility of monolayer adsorption and homogeneous surface. Halsey and R-P isotherms were found second and third most suitable isotherms after Freundlich.

The values of R-P isotherm constants (β) were 0.43, 0.46, 0.53 and 0.74, 0.71, 0.74 for RH and FeRH, respectively at 20, 35 and 50 ºC. These values were between 0 to 1, which indicated that the data was well fitted and adsorption of Cr (VI) took place in multilayer fashion on RH and FeRH surface. Similarly, Saha et al., 2013 also reported multilayer adsorption of Cr (VI) ions on heterogeneous surface of *Citrus limetta* peels.

4.7.3.0 Thermodynamics

Thermodynamic functions (ΔS^o and ΔH^o) are calculated from intercept and slope of the plot between ln K_c and 1/K (Figure 4.12).

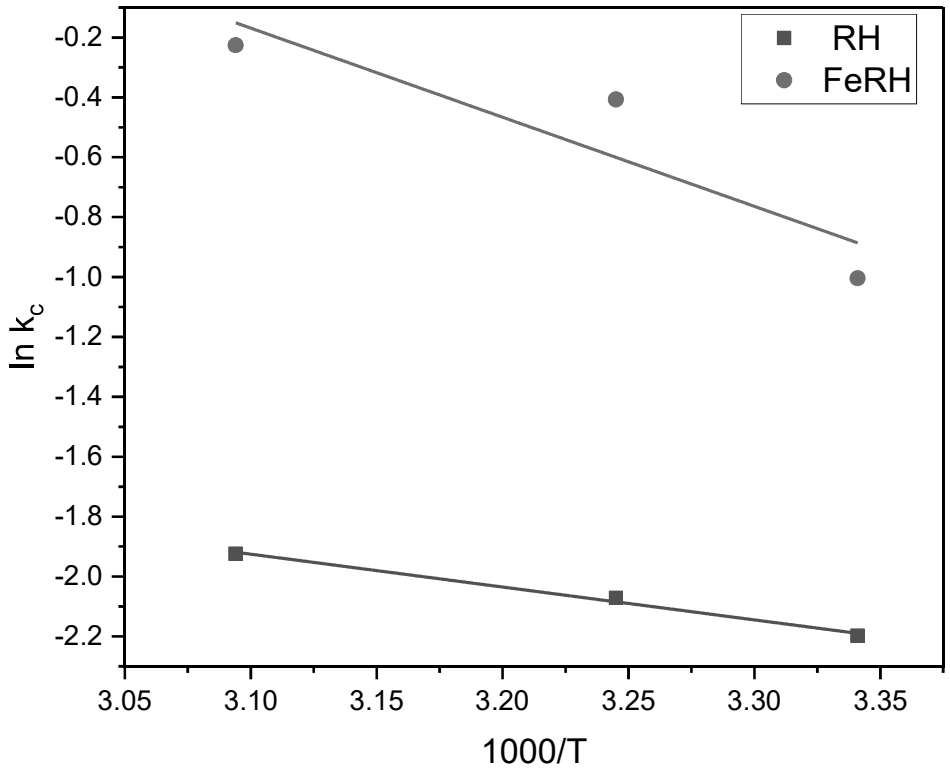

Figure 4.12 Thermodynamic study of Cr (VI) adsorption onto RH and FeRH

The thermodynamic parameters were calculated and are tabulated in Table 4.5.

Table 4.5 Thermodynamic parameters

Temperature (°K)	**ΔG° (kJ mol^{-1})**	**ΔH° (kJ mol^{-1})**	**ΔS° (kJ mol^{-1} K^{-1})**
RH			
293.15	-5357.62		
308.15	-5307.03	1.09719	1.47593
323.15	-5169.55		
FeRH			
293.15	-2544.79		
308.15	-1045.19	2.97561	9.05563

323.15	-609.60

The positive ΔH^o for the RH and FeRH specified endothermic adsorption. The positive ΔS^o and negative ΔG^o designated favourable and spontaneous adsorption of Cr (VI). Yusuff, 2019 reported similar kinds of results for Cr (VI) removal onto *Leucaena leucocephala* seed pod activated carbon. Gorzin and Abadi, 2017 performed Cr (VI) adsorption onto adsorbent prepared from paper mill sludge and results were similar to the present investigation. Saha et al., 2013 also performed the Cr (VI) adsorption on *Citrus limetta* peels powder and recorded that adsorption was spontaneous and endothermic.

4.7.4 Adsorption kinetics

PFO, PSO and Elovich kinetic models are shown in Figure 4.13.

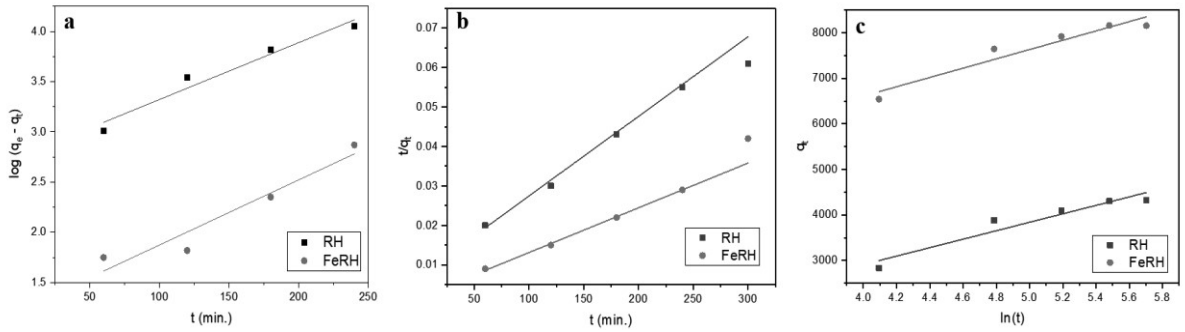

Figure 4.13 PFO (a), PSO (b) and Elovich kinetic (c) of Cr (VI) adsorption of RH and FeRH

The values of kinetic model parameters are tabulated shown in Table 4.6.

Table 4.6 Kinetic model constants and error functions

PFO					
	K_s	Q_e	R^2	*SSE*	χ^2
RH	0.005	2.87	0.98	1.39	0.34
FeRH	0.007	0.98	0.97	1.72	0.43

PSO					
	H	k_2'	R^2	SSE	χ^2
RH	1.78	0.009	0.99	0.002	0.0005
FeRH	1.33	0.012	0.99	0.013	0.0032

Elovich					
	a	β	R^2	SSE	χ^2
RH	928.71	-805.11	0.91	122133.6	30533.4
FeRH	1021.01	2526.06	0.92	127129.9	31782.4

The greater R^2 and lower error (SSE and χ^2) echoed that PSO had a better fit in comparison to other kinetic models. Sun et al., 2020a reported that PSO better fitted in Cr (VI) removal data by using tannin based biosorbent compared to PFO. Kumar et al., 2020 did Cr (VI) biosorption onto chemically modified *Datura stramonium* fruit and reported that PSO was suitable to explain biosorption.

4.7.5 Mechanistic study

The values of mechanistic parameters are shown in Table 4.7.

Table 4.7 Mechanistic parameters

IPD					
	K_{id}	C	R^2	SSE	χ^2
RH	149.97	1939.75	0.84	236219.03	59054.75
FeRH	165.46	5534.74	0.85	253960.03	63490.00
LFD					

	F	K_{fd}	R^2	SSE	χ^2
RH	-0.02	0.53	0.93	0.72	0.18
FeRH	-0.02	0.45	0.89	1.74	0.43

Bangham's model

	α	K_i	R^2	SSE	χ^2
RH	0.32	-1.39	0.89	0.36	0.29
FeRH	0.29	-0.83	0.84	0.15	1.03

LFD model showed better goodness of fit with highest R^2 and lowest SSE as compared to IPD and Bangham's model. The LFD coefficient (K_{fd}) values were found to be 0.5375 $\mu g g^{-1} min^{-1}$ and 0.4525 $\mu g g^{-1} min^{-1}$. The non-zero value of K_{fd} complemented the fact that adsorption of Cr (VI) ion on FeRH and RH was film diffusion dependent. Maremeni et al., 2018 also reported that LFD was rate controlling step in adsorption of Cr (VI) on nut shell powder. Pholosi et al., 2020 reported similar kind of observations in Cr (VI) adsorption onto magnetite pine composites. Song et al., 2016 investigated Cr (VI) adsorption onto wheat straw and *Eupatorium adenophorum* and reported similar kinds of results.

In the present study, the values of D_f were 1.14×10^{-7} cm^2 s^{-1} and 4.34×10^{-7} cm^2 s^{-1} for RH and FeRH. The D_p was found to be 8.8×10^{-10} cm^2 s^{-1} and 1.32×10^{-10} cm^2 s^{-1} for RH and FeRH. The results are in the suggested range of D_f (10^{-6} to 10^{-18} cm^2 sec^{-1}). The values of D_f boomed that the adsorption of Cr (VI) ions on the RH and FeRH was film diffusion limited.

4.8.0 Assessment of adsorption capacities

Comparative analysis of various other adsorbents in terms of their Cr (VI) uptake capacity is shown in Table 4.8.

Table 4.8 Cr (VI) uptake capacities of RH and FeRH and other adsorbents.

Adsorbent	**Uptake capacity (mg/g)**	**pH**	**Temperature (°C)**	**Adsorbent dose (g/L)**	**Initial conc. (mg/L)**	**References**
Opuntia biomass	16.5	2	20	0.5	10	[Fernandez-Lopez, 2014]
Cotton waste	6.75	2	25	3	20	[Boosaeidi et al., 2017]
Barberry waste	7.89	2	25	5	40	[Boosaeidi et al., 2017]
Macadamia nutshell powder	45.23	2	--	0.5	100	[Pakade et al., 2017]
Oedogoniu m hatei biomass	31	2	45	0.8	50	[Gupta et al., 2009]
Oedogoniu m hatei biomass (Acid treated)	35.2	2	45	0.8	100	[Gupta et al., 2009]
Barks of *Acacia albida*	2.98	2	37	20	7.5	[Gebrehawaria et al., 2015]

Leaves of *Euclea schimperi*	3.94	2	37	20	7.5	[Gebrehawaria et al., 2015]
Macadamia nutshell powder (modified)	72.12	2	--	2.5	150	[Maremeni et al., 2018]
Aspergillus niger NU101 Biomass	17.58	6	30	2	25	[Ghosh et al., 2015]
Dictyota dichotoma biomass	9.02	4	27	20	40	[Nandhagopal et al., 2018]
RH	6.88	2	50	5	50	*Present study*
FeRH	11.14	2	50	5	50	*Present study*

Certainly, FeRH possesses extensive potential of Cr (VI) uptake like most of the adsorbents cited in Table 8 and this was attributed to the surface morphological structure, functional groups and doped ferrous ions on the surface of RH.

Though FeRH has high Cr (VI) uptake capacity (11.14 mg/g) which removes 81.56 % Cr (VI) from aqueous solution containing 50 mg/L initial Cr (VI) concentration in first round, yet 9.22 mg/L Cr (VI) is left in the liquid phase. This remaining Cr (VI) in the water is much higher than the permissible limit of discharge. Hence, the remaining Cr (VI) was removed through the re-circulation of 1st reactor's treated metal ion solution into second reactor added

in series. 100% removal of Cr (VI) is obtained after second stage of treatment, this meets with the prescribed limits of discharge. The detailed experimental setup is shown in Figure 4.14.

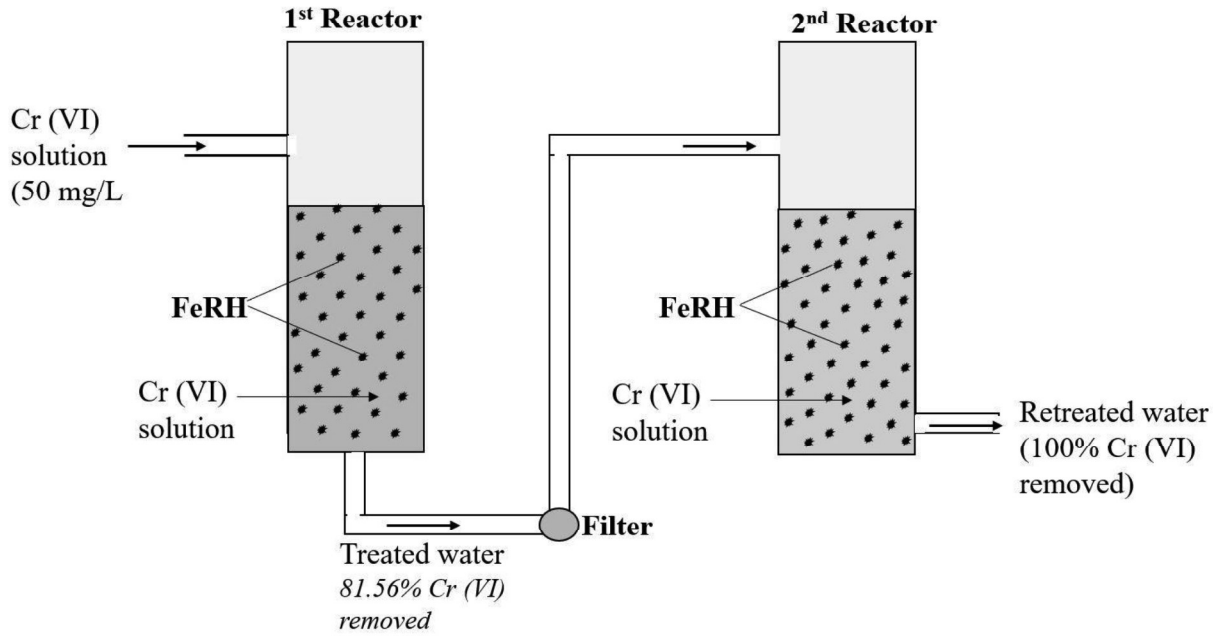

Figure 4.14 Diagrammatic representation of Cr (VI) removal

4.9.0 Recovery of FeRH

The regeneration of FeRH was carried out using 0.1 N HNO_3 as eluent. The sequences of adsorption and desorption are shown in Figure 4.15.

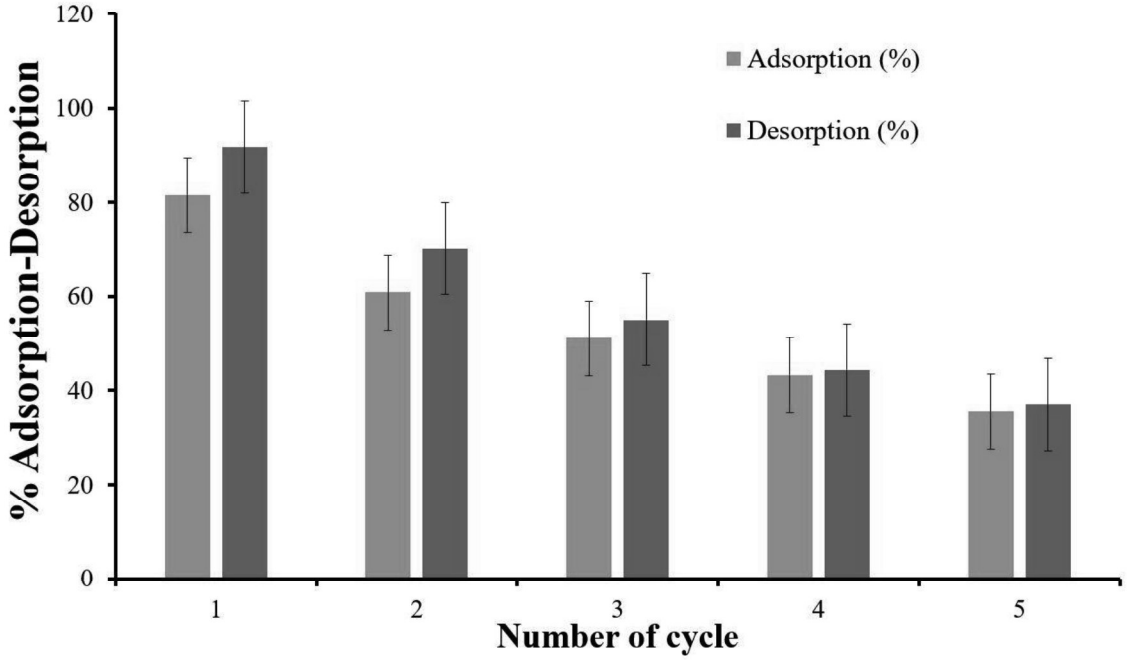

Figure 4.15 Sequences of Cr (VI) adsorption and desorption

There was a decrement in adsorption of Cr (VI) on FeRH from 81.56 to 35.53% in five consecutive sequences of adsorption and desorption. Repetitive washing, elution and incapability of eluting reagent in desorbing adsorbed Cr (VI) ions resulted in depreciation in weight and deactivation of active sites of FeRH. The efficiency of desorption ranged from 91 to 37.03% but 100% was not achieved. The sturdy binding (chemisorptive) of Cr (VI) with FeRH was reason behind this. Patra et al., 2019 reported that there was a steady reduction in Cr (VI) adsorption on untreated, acid modified and chelated *Sterculia villosa* Roxb in six consecutive sequences of adsorption and desorption. Similarly, Chen et al., 2019 recorded a slow but sure decline in adsorption of Cr (VI) ion in six repeated series of adsorption and desorption.

4.10 Techno-economic analysis

The cost analysis is a primary approach of scaling up the heavy metal treatment process [Santos-Juanes Jorda et al., 2011; Fawzy et al., 2018]. The cost estimation assists in the design water treatment systems [Hamdy et al., 2018]. In the present study the production cost of adsorbent (FeRH) was estimated. The operation cost per cubic meter of water treatment was calculated through sum of chemicals/reagents and biosorbent cost. The cost/price of adsorbent (Pi) is calculated as;

P_i ($USD/g) = Raw materials cost + chemicals/regents + adsorbent preparation cost

The operation cost for treatment of heavy metal ions was calculated using following Equation

$$\text{Operation cost } (\$USD/m^3) = C_i \times P_i$$

Where C_i (g/m^3) is the concentration of adsorbent and P_i ($USD/g) is price of adsorbent.

In this present study, the cost of FeRH was calculated as 0.27 $USD/g which used for the removal of Cr (VI) from water and 5 g FeRH used for the treatment of 1 litre of water. The operation cost of FeRH mediated Cr (VI) treatment was calculated using Equation 37 and observed 1350 $USD/$m^3$. Fawzy et al., 2019 prepared adsorbent using Olive leaves for removal of Cr (II) and investigated techno-economic value. Authors reported similar kind of results in their research.

4.11 Conclusion

In the present study, the ecofriendly and cost effective methods have been proposed for removal of Cd (II), Cr (VI) and Pb (II) from water. Physico-chemical characterization of FeRH showed the presence of -OH and -NH groups on its surface together with rough texture with high carbon content and large BET surface area. The coating of iron and the successful reduction of Cr (VI) to Cr (III) on FeRH surface was observed. Cr (VI) adsorption was chemisorptive, favourable, endothermic, spontaneous, multilayer in nature and diffusion limited. FeRH showed high chromium desorption which indicated that FeRH is applicable in

multiple adsorption-cum-reduction cycle of Cr (VI). Acidic pH_{zpc} indicated potential application of FeRH in industrial effluents like spent pickling acid and acid mine drainage.